Tectonophysics 518–521 (2012) 55–62

Contents lists available at SciVerse ScienceDirect

Tectonophysics

journal homepage: www.elsevier.com/locate/tecto

Crustal deformation and kinematics of the Eastern Part of the North Anatolian Fault Zone (Turkey) from GPS measurements

Orhan Tatar [a,*], Fatih Poyraz [b], Halil Gürsoy [a], Ziyadin Cakir [c], Semih Ergintav [d], Zafer Akpınar [a], Fikret Koçbulut [a], Fikret Sezen [a], Tarık Türk [b], Kemal Ö. Hastaoğlu [b], Ali Polat [a], B. Levent Mesci [a], Önder Gürsoy [e], İ. Ercüment Ayazlı [f], Rahşan Çakmak [d], Alpay Belgen [d], Hakan Yavaşoğlu [e]

[a] Cumhuriyet Üniversitesi, Jeoloji Mühendisliği Bölümü, 58140 Sivas, Turkey
[b] Cumhuriyet Üniversitesi, Geomatik Mühendisliği Bölümü, 58140 Sivas, Turkey
[c] Istanbul Teknik Üniversitesi Maden Fakültesi Jeoloji Mühendisliği Bölümü, Istanbul, Turkey
[d] TÜBİTAK-MAM Yer ve Deniz Bilimleri Enstitüsü, Gebze-Kocaeli, Turkey
[e] İstanbul Teknik Üniversitesi İnşaat Fakültesi Geomatik Mühendisliği Bölümü, Istanbul, Turkey
[f] Yıldız Teknik Üniversitesi İnşaat Fakültesi, Harita Mühendisliği Bölümü, Istanbul, Turkey

ARTICLE INFO

Article history:
Received 28 July 2011
Received in revised form 1 November 2011
Accepted 5 November 2011
Available online 13 November 2011

Keywords:
North Anatolian Fault Zone
Crustal deformation
GPS velocities
Slip rate
Eastern Turkey

ABSTRACT

The North Anatolian Fault Zone (NAFZ) is a 1200 km long dextral strike-slip fault zone forming the boundary between the Eurasian and Anatolian plates. It extends from the Gulf of Saros (North Aegean) in the west to the town of Karlıova in eastern Turkey. Although there have been numerous geodetic studies concerning the crustal deformation, velocity field and the slip rate of the NAFZ along its western and central segments, geodetic observations along the eastern section of the NAFZ are sparse. In order to investigate the GPS velocities and the slip rate along the eastern part of the NAFZ, a dense GPS network consisting of 36 benchmarks was installed between Tokat and Erzincan on both sides of the fault zone and measured from 2006 to 2008.

Measurement results indicate that the slip rate of the NAFZ increases westwards within about 400 km from 16.3 ± 2.3 mm/year to 24.0 ± 2.9 mm/year, in consistence with the observation that the Anatolian block is being pulled by the Hellenic trench rather than being pushed by the Arabian plate as a result of continental collision between the Arabian and Eurasian plates in eastern Turkey since late Miocene. Modelling the GPS velocities shows that fault locking depth increases also in the same direction from 8.1 ± 3.3 km to 12.8 ± 3.9 km. Slip rate decreases as moving off the Hellenic trench. An average slip rate of 20.1 ± 2.4 mm/year and a locking depth of 12.5 ± 3.5 km are also estimated for the entire study area by using all of the GPS measurements obtained in this study. The GPS velocities are in good agreement with the kinematic models created by paleomagnetic studies in the region and complete the overall picture.

1. Introduction

Forming the boundary of the Eurasian and Anatolian tectonic plates, the North Anatolian Fault Zone (NAFZ) is one of the major strike-slip fault zones of the world. The 1200 km-long NAFZ runs along the northern part of Turkey, roughly parallel to the Black Sea from Karlıova in the east to the Gulf of Saros in the west, connecting the East Anatolian compressional region to the Aegean extensional region. The study area where the NAFZ and East Anatolian Fault Zone (EAFZ) meet at Karlıova triple junction in Eastern Turkey, comprises a complicated combination of active plate boundaries (Fig. 1). Şengör et al. (1985) and Dewey et al. (1986) hypothesized that, due to the northward movement of the Arabian plate relative to Eurasia, the Erzincan–Karlıova region is squeezed, crushed, and expelled westward along the NAFZ and EAFZ. As a result of this plate convergence, right-lateral strike-slip faulting along the NAFZ (Dewey and Şengör, 1979; McClusky et al., 2000; Şengör, 1979) and left-lateral strike-slip faulting along the EAFZ (Jackson and McKenzie, 1988; McKenzie, 1972; Tatar et al., 2004) in eastern Turkey accommodates the westward motion of Anatolia relative to Eurasia. GPS observations over the last two decades however reveal that slab pull along the Hellenic trench is now more important than the push by the collision in eastern Turkey (McClusky et al., 2000; Oral, 1994; Reilinger et al., 1997, 2006).

In general, the NAFZ becomes wider from east to west (Şengör et al., 2005). While the zone is generally extremely narrow, hardly wider than 10 km, (Herece and Akay, 2003) between Karlıova triple junction and Niksar basin (Fig. 2) in eastern Turkey it becomes a

* Corresponding author at: Çanakkale Onsekiz Mart Üniversitesi, Jeoloji Mühendisliği Bölümü, 17100 Çanakkale, Turkey. Tel.: +90 532 615 3898; fax: +90 286 218 0541.
E-mail addresses: orhantatar@cumhuriyet.edu.tr, orhantatar@comu.edu.tr (O. Tatar).

0040-1951/$ – see front matter © 2011 Elsevier B.V. All rights reserved.
doi:10.1016/j.tecto.2011.11.010

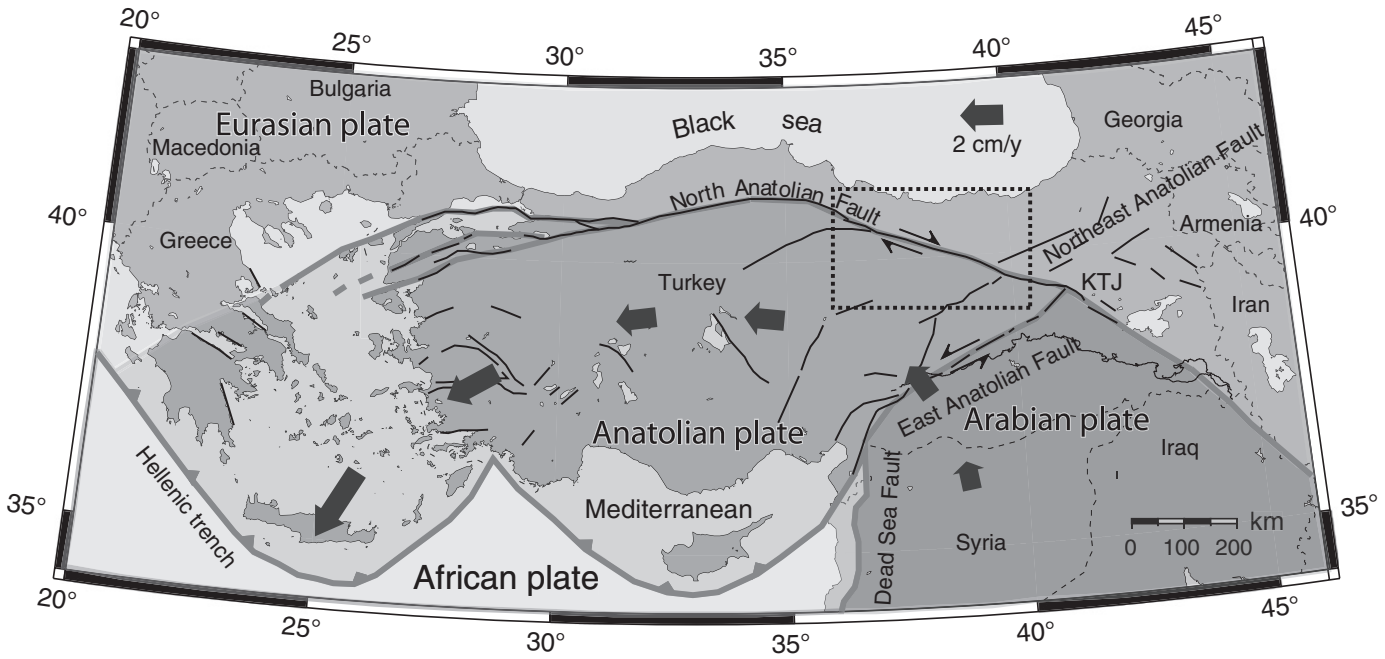

Fig. 1. Tectonic setting of Turkey and surrounding regions. Arrows show the anticlockwise rotation of the Arabian and Anatolian plates with respect to the Eurasian reference frame increasing westward (after McClusky et al., 2000). Thin black lines are active faults (from Şaroğlu et al., 1992). Dashed rectangle shows the location of study area along the North Anatolian Fault (KTJ = Karlıova Triple Junction).

shear zone of a few hundred km wide around the Marmara region in northwest Turkey. The long-term geological slip rates have been estimated between 10 mm/year and 20.5 mm/year along different segments of the NAFZ, based on different geological, seismological and paleomagnetic methods (Barka and Kadinsky-Cade, 1988; Kasapoğlu and Toksöz, 1983; Kiratzi and Papazachos, 1995; Kozacı et al., 2007; Pınar et al., 1996; Piper et al., 1997; Tatar et al., 1995; Taymaz et al., 1991). The dextral shear is not confined to the NAFZ but is distributed in a broader shear zone as confirmed by paleomagnetic observations indicating clockwise rotations of up to 270° within the past 5 Ma in the central parts of NAFZ (Piper et al., 1997, 2006, 2009; Tatar et al., 1995). Where observations are made in the central part of the NAFZ, the shear-related clockwise rotations are found in areas as far south as 25 km from the main strand of the NAFZ in contrast to earlier reports of no rotation by Platzman et al. (1994). However, the rotations within the NAFZ are not found to be systematic, possibly because of the early activity of R shears (Piper et al., 1996; Şengör et al., 2005). Farther west, around the western half of the Sea of Marmara, rotations of Miocene and younger units are spread over a width of more than 100 km (Tapırdamaz and ve Yaltırak, 1996). In this region, the rotations are also very complex, indicating a complicated strain history in keeping with the expected evolution of a broad shear zone (Şengör et al., 2005). By contrast, in the eastern part of the NAFZ, the rotations are confined to a much narrower shear zone of some 15 km wide (Tatar et al., 1995).

The present day short-term slip rates obtained by recent geodetic measurements along the central and western segments of the NAFZ are estimated to be between 28 mm/year and 24 mm/year, notably faster than the long-term geological slip rates (Straub, 1996). The slip rate reported by McClusky et al. (2000) is 22–24 ± 1 mm/year for the NAFZ, from the Euler pole estimation, where as Reilinger et al. (2006) estimated a slightly higher slip rate, 25 mm/year, based on block modelling. They used the same data set and represent the average value from Erzincan, in the east, to Bolu, in the west (Fig. 2). It is obvious that the detailed studies should be run to

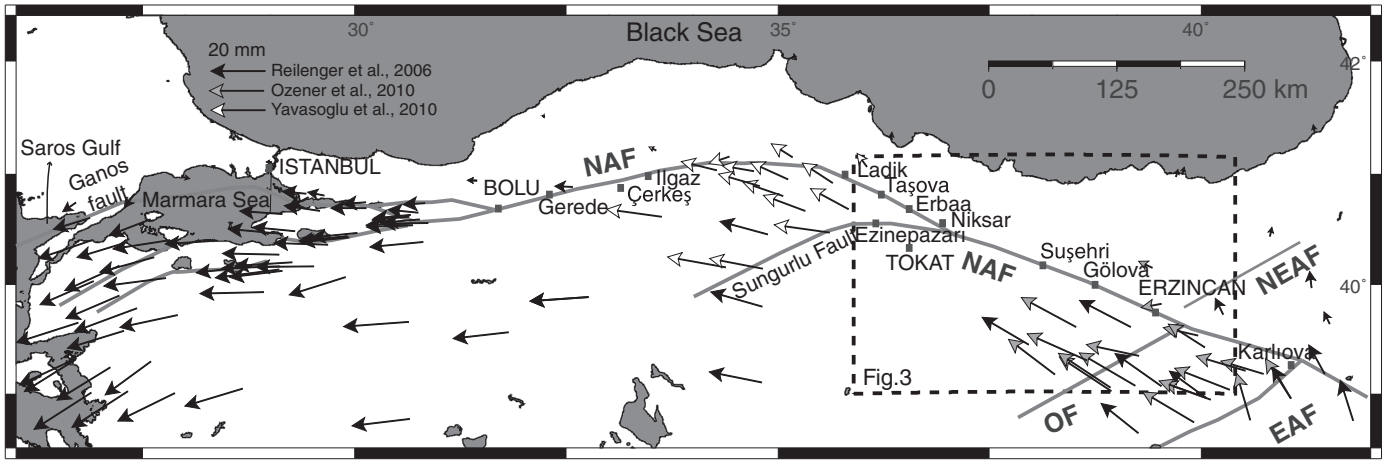

Fig. 2. GPS velocities along the North Anatolian Fault Zone (NAFZ) from various studies (OF = Ovacık fault; EAF = East Anatolian Fault; NEAF = Northeast Anatolian Fault). Note the gap in the velocity field between Erzincan and Ladik. Rectangle with dashed lines shows the location of Fig. 3.

estimate the slip rates along different segments of NAFZ. Therefore, Yavaşoğlu et al. (2011) established a local GPS network along the central part of the North Anatolian Fault Zone between Ladik and Ilgaz (Fig. 2) and estimated slip rates ranging between 18.7 ± 1.6 and 21.5 ± 2.1 mm/year after five years of observations. As shown in Fig. 2, there is a significant gap in the GPS network along the eastern segments of the NAFZ between Erzincan and Erbaa (Tokat). Therefore, we have established a new GPS network along this section of the NAFZ and measured it for 3 years. The study area has experienced intense and devastating earthquakes during the years of 1939, 1942 and 1992. The NAFZ, Northeast Anatolian Fault (NEAF) and Ovacık Fault (OF) are the most important regional tectonic features of the region in which several strike-slip related sedimentary basins such as Erzincan, Suşehri, Gölova, Niksar, Erbaa-Taşova, have formed (Figs. 1 and 2). The abundance of historical earthquakes is very much related with the movements of these three main faults (Kaypak and Eyidoğan, 2002). The December 26th 1939 Erzincan earthquake is the strongest earthquake ever recorded in Turkish history (Mw = 7.9), which produced a 360-km-long surface break between Erzincan to Ezinepazarı (Ketin, 1976) bounding the Erzincan, Suşehri and Niksar basins (Barka and Kadinsky-Cade, 1988). The 1939 Erzincan earthquake was followed, in rapid succession, by a series of disastrous earthquakes in Niksar-Erbaa in 1942 (Ms = 7.1); in Ladik in 1943 (Ms = 7.3); and in Bolu, Gerede, and Çerkeş in 1944 (Ms = 7.3). On December 20th 1942, a destructive earthquake with a magnitude of 7.2 occurred around Erbaa and Niksar and created a new 50 km long surface break bounding the northern margin of the Niksar pull-apart basin (Tatar, et al., 2006).

2. Data collection and processing

2.1. GPS measurements

Monitoring tectonic movements in this region is a challenging task for various reasons and, a dedicated geodetic network for geodynamic purposes was constructed (Fig. 3). GPS stations were built into bedrock using high quality geodetic monuments. Observations were performed at each station for three sections of 10 hours per day during 3 years between 2006 and 2008. Additionally, other available GPS sites nearby, having a longer data span, have been included in the present analysis. Observation spans of GPS sites used in this study are summarised in Table 1.

GPS velocities are determined for 42 stations, 36 measured with survey-mode GPS (SGPS) in the study area (i.e., including six global stations in the analysis). GPS measurement campaigns were conducted between July and August in order to minimize annual seasonal systematic errors. To reduce the antenna phase pattern problems and the errors on the computation of the vertical components, we used the same receivers and antennas at all campaign sites (Trimble 4000 and 5700 with choke-ring and geodetic Zephyr antennas).

2.2. GPS data processing

The GPS data were processed with the GAMIT/GLOBK software (Herring et al., 2006a,b). In general, measurements processed in three phases with using GAMIT/GBLOK (Dong et al., 1998; Feigl et al., 1993; McClusky et al., 2000; Oral, 1994). At the first step, daily observations of doubly differenced GPS phase were used to estimate the coordinates of observation points, atmospheric zenith delays of each observation point and Earth Orientation Parameters (EOPs). 6 International GPS Service (IGS) stations were included within the analysis to create a link between regional and global networks as overlapping "tie" sites and combined solutions were obtained in order to use the precise IGS products.

At the second step, Kalman Filter is to be implemented according to EOP values, orbit data daily coordinates and covariance to estimate the site coordinates and velocities from the combined solutions. In the last step, the reference frame was constrained on each day using a reliable set of global IGS stations with respect to the IGS00 realization

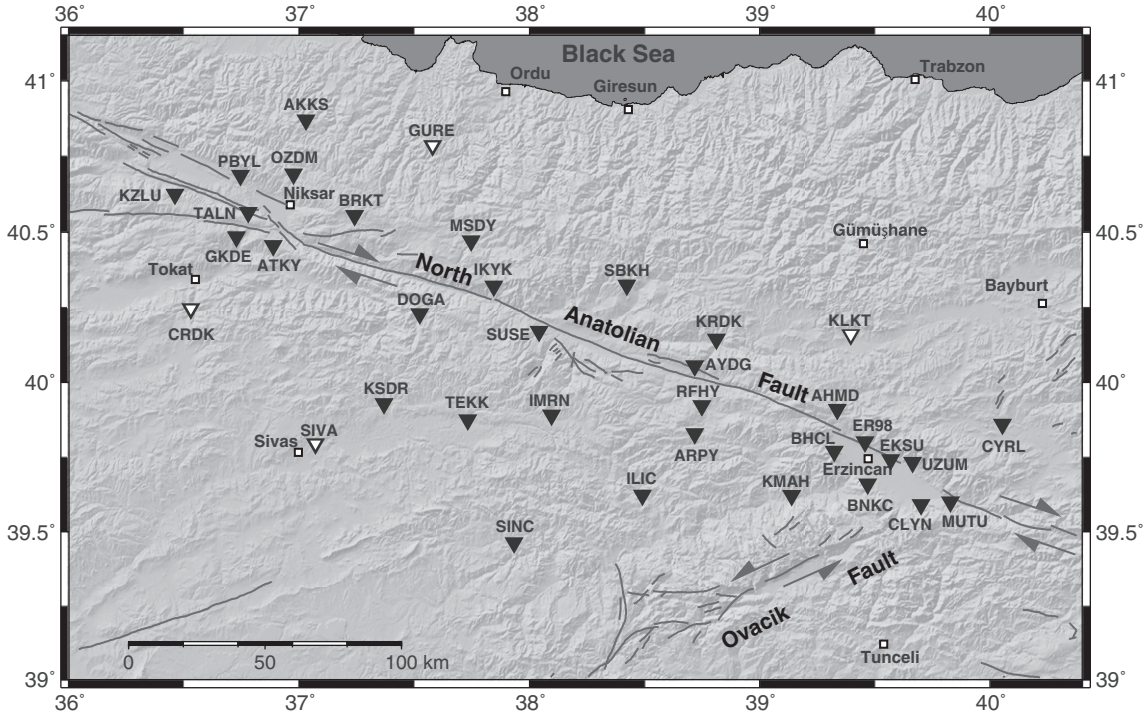

Fig. 3. The GPS bench marks constructed in this study along the eastern NAFZ. 4 of 36 GPS sites were permanent (white inverted triangles) during 2006–2008 GPS campaigns and located on both sides of the NAFZ in Kelkit (KLKT), Gürgentepe (GURE), Sivas (SIVA) and Tokat (CRDK).

Table 1
Horizontal GPS velocities of the Kelkit Region with respect to the Eurasian fixed frame and 1-sigma uncertainties (plotted with 95% confidence ellipses in Fig. 4).

SITE	Longitude (θ)	Latitude (θ)	E&N Rate (mm/year)		E&N 1-sigma uncertainties (mm/year)		RHO
CYRL	40.079	39.852	−5.71	2.73	0.52	0.65	−0.086
MUTU	39.853	39.591	−13.11	8.17	0.54	0.67	−0.089
CLYN	39.725	39.582	−12.19	9.56	0.54	0.67	−0.084
UZUM	39.688	39.724	−11.36	3.56	0.54	0.67	−0.083
EKSU	39.593	39.733	−10.52	3.37	0.57	0.73	−0.098
BNKC	39.494	39.652	−15.59	5.35	0.82	1.07	−0.055
ER98	39.482	39.793	−10.52	0.77	0.52	0.64	−0.083
KLKT	39.420	40.151	−4.55	1.60	0.27	0.26	−0.034
AHMD	39.361	39.902	−4.24	−1.26	0.52	0.64	−0.090
BHCL	39.349	39.762	−13.57	3.37	0.61	0.77	−0.078
KMAH	39.164	39.613	−10.87	7.71	0.47	0.57	−0.088
KRDK	38.836	40.136	−4.09	2.70	0.49	0.61	−0.092
RFHY	38.774	39.914	−13.87	5.92	0.44	0.54	−0.081
ARPY	38.743	39.820	−18.39	9.60	0.45	0.53	−0.082
AYDG	38.743	40.047	−10.58	0.12	0.51	0.64	−0.088
ILIC	38.515	39.614	−11.76	8.02	0.48	0.58	−0.092
SBKH	38.448	40.316	−5.05	−1.70	0.46	0.55	−0.087
IMRN	38.121	39.882	−13.35	7.48	0.55	0.69	−0.108
SUSE	38.067	40.162	−14.74	7.03	0.55	0.68	−0.102
SINC	37.958	39.454	−18.18	9.88	0.50	0.58	−0.068
IKYK	37.869	40.313	−7.74	4.87	0.45	0.53	−0.082
MSDY	37.771	40.463	−4.46	4.98	0.46	0.54	−0.067
TEKK	37.757	39.867	−18.82	10.13	0.46	0.56	−0.101
GURE	37.604	40.778	−2.12	1.41	0.26	0.24	−0.027
DOSA	37.549	40.221	−17.47	7.73	0.41	0.48	−0.085
KSDR	37.394	39.921	−21.28	5.96	0.45	0.54	−0.090
BRKT	37.265	40.547	−9.09	5.18	0.41	0.48	−0.090
SIVA	37.095	39.786	−20.33	8.58	0.26	0.24	−0.035
AKKS	37.054	40.863	−1.13	−0.85	0.43	0.53	−0.104
OZDM	37.001	40.685	−5.48	4.07	0.45	0.55	−0.088
ATKY	36.912	40.447	−19.95	6.09	0.97	1.28	−0.088
TALN	36.804	40.557	−13.52	5.23	0.48	0.57	−0.103
PBYL	36.770	40.680	−5.77	3.12	0.41	0.48	−0.090
GKDE	36.752	40.476	−14.42	6.74	0.45	0.54	−0.097
CRDK	36.554	40.237	−20.73	7.08	0.25	0.23	−0.032
KZLU	36.485	40.617	−17.18	4.80	0.39	0.46	−0.095
POL2*	74.694	42.680	−0.07	0.88	0.12	0.12	−0.028
KIT3*	66.885	39.135	−0.69	0.94	0.14	0.13	−0.039
METS*	24.395	60.217	0.03	−1.09	0.14	0.16	0.049
JOZE*	21.032	52.097	−0.33	1.30	0.19	0.22	−0.014
TROM*	18.938	69.663	−0.17	1.00	0.12	0.14	0.090
GRAZ*	15.493	47.067	0.26	0.73	0.13	0.14	−0.025
POTS*	13.066	52.379	−0.78	−0.21	0.11	0.12	0.009
WTZR*	12.879	49.144	−0.48	−0.30	0.13	0.15	0.007
ZIMM*	7.465	46.877	0.51	1.36	0.14	0.15	0.042
KOSG*	5.810	52.178	0.53	−0.05	0.19	0.23	0.022
BRUS*	4.359	50.798	0.29	−0.68	0.12	0.14	0.044
HERS*	0.336	50.867	−0.06	−0.14	0.12	0.13	0.050

Latitude and longitude are given in degrees North and East, respectively. Station velocities and their uncertainties are given in mm/year. (*) The Eurasian frame is determined by minimizing the adjustment to the horizontal velocities of the 12 stations given at the end of table. RHO is the correlation coefficient between the E (east) and N (north) uncertainties.

of ITRF2000 no-net-rotation (NNR) frame (ITRF2000I) (Ray et al., 2004), while estimating the translation, orientation and scale parameters for each day with the origin fix module (GLORG) of GLOBK. Details about the processing method are described in McClusky et al. (2000).

We defined a Eurasian frame by minimizing the horizontal velocities of 12 IGS stations. All of them have long reliable times series and selected after the several alternative realizations of reference frame using different subset of the stations, distributed between Western Europe to Central Asia, based on the root-mean-square departure of the velocities. The root-mean-square departure of the velocities of the 12 stations after transformation was 0.3 mm/year. Velocities of stations in Eastern NAFZ GPS network (Turkey) with respect to Eurasia are shown in Fig. 4 and listed in Table 1.

3. General view of the processing results

Fig. 4 shows the GPS velocity field with respect to fixed Eurasian reference frame we have deduced from our network in this study. The GPS vectors on the Anatolian block are pointing NW direction nearly parallel to the NAFZ, indicating that this section of the NAFZ has pure strike-slip mechanism. The amplitude of the vectors increases from north to south, consistent with a locked right-lateral strike-slip fault. At SIVA and SINC sites located further south velocities are calculated as 22 mm/year and 21 mm/year respectively. At the northern part of the fault zone, the GPS velocities are ranging between 1–6 mm/years and around 6–10 mm/year closer to the fault zone. Velocity values are decreasing away from the fault to the north and values become closer to zero gradually. GURE station is located furthest north and the value obtained from this point is 4 mm/year demonstrating the wideness of deformation on Eurasian plate as well as the behaviour of elastic deformation affecting a large zone along the plate boundary in the region.

An increase in velocity is evident also from east to west at the GPS sites located on the southern side of the fault zone. While the rates are around 13–15 mm/year at MUTU and KMAH in the east, they are 20–22 mm/year at SIVA, CRDK and SINC site towards the west.

4. Interpreting and modelling the GPS data

Relative velocity between the Anatolian and Eurasian plates and the locking depth along the NAFZ in the study area (Fig. 1) can be estimated from the GPS data using the model proposed by Savage and Burford (1973) in which the accumulation of strain along a strike-slip fault is described by a buried screw dislocation in elastic half-space (Fig. 5). According to this two dimensional model, the uppermost portion of the fault is locked due to friction between earthquakes, where as the lower part creeps continuously at a constant rate equal to the rate of relative plate motion (Fig. 4a). For an infinitely long, planar and vertical strike-slip fault locked from surface down to a depth of d (i.e., locking depth) the fault-parallel velocity (v) as a function of position (x) orthogonal to the fault is given by

$$v(x) = \frac{v_p}{\pi} - \tan^{-1}\frac{x}{d}$$

where v_p is creeping rate of the deep fault below the locking depth (d) that is equal to the rate of plate velocity in the far field, and is often termed as slip rate, in which case it is assumed that crust is purely elastic and hence all the accumulated strain in the locked section of the fault is released coseismically. Fig. 5b shows plots of this function for varies locking depths, illustrating that while the steady state deep creep determines the difference in the far field velocity across the fault (i.e., the limits of velocity axis), the slope of the curve around the fault is controlled by the locking depth. Note that the velocity profile is symmetric about the fault as the model assumes an idealized and isotropic rheology for the Earth's crust and a vertical fault plane (Fig. 5b). Despite its simplicity the 2D screw dislocation model has been used in many crustal deformation studies and has proven to work quite well in producing the overall pattern of deformation observed at transform fault boundaries (Alchalbi et al., 2010; Cakir et al., 2005; Ergintav et al., 2007; Motagh et al., 2007; Segall, 2002)

To model the GPS data we construct three fault-perpendicular profiles, each 100 km apart between Tokat and Erzincan (Fig. 4). In each profile, the fault-parallel (N70°W) components of all GPS vectors within a distance of 100 km are projected on to the profile and plotted with %95 confidence error bars (Fig. 6). Four parameters are estimated form the GPS profiles: slip rate (in other words deep

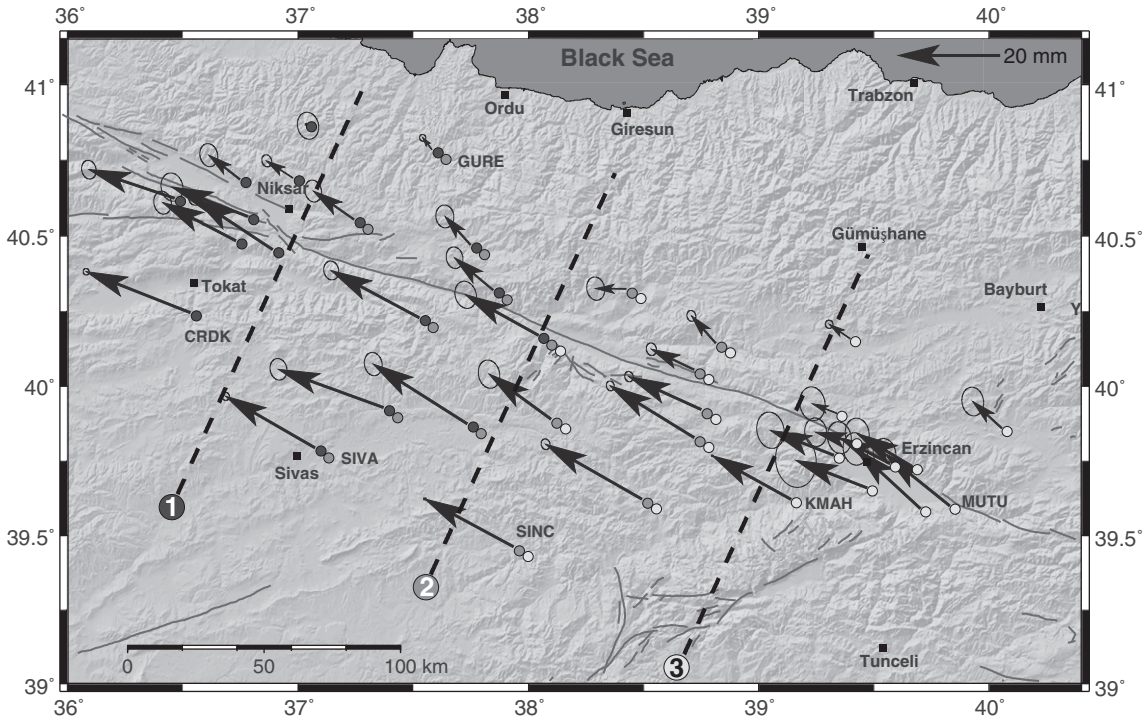

Fig. 4. GPS velocity field of the study area with respect to Eurasian reference frame with error ellipses within 95% confidence region on a shaded SRTM elevation model (Farr et al., 2007). Gray lines are active faults in the region (from Şaroğlu et al., 1992). Black dashed lines are profiles perpendicular to the NAFZ with about 100 km spacing. GPS vectors projected onto each profile are indicated by small circles with a different colour at their tails.

creep or secular velocity of the region) (v_p), locking depth (d), shift (horizontal) in fault position along profile (s_h), and shift (vertical) in reference point for velocity (s_v). To estimate these parameters, we use (following Segall, 2002) a modified bootstrap procedure. At first step, for each fixed distance (x_i) along the profile, we compute the corresponding predicted velocity, $\hat{v}_i = f\left(x_i, \hat{\theta}\right)$ for model $i = 1, 2, \ldots, n$ where $\hat{\theta} = \left(\hat{v}_p, \hat{d}, \hat{S}_h, \hat{S}_v\right)$. Then the corresponding residuals ($\hat{e}_i = v_i - \hat{v}_i$) estimated for $i = 1, 2, \ldots, n$. To correct for the potential heteroscedastic residual variances, the residuals are modified ($, r_i = \hat{e}_i / \sqrt{1-h_i}$), and centred ($r_i - \bar{r}$) for $i = 1, 2, \ldots, n$. Hence, we built a random n sample group and update the fitted $\hat{v}_i$–values with resampled residuals in order to generate a bootstrap sample of v-values corresponding to the original fixed x-values. Using a Levenberg–Marquadt nonlinear optimization algorithm with no priori bounds, the parameters are estimated within %95 confidence limits (Arnadottir and Segall, 1994; Motagh et al., 2007). Bootstrap standard errors and confidence limit are estimated from the 500-parameter estimates.

Modelling results indicate that the slip rate of the NAFZ increases westwards within about 400 km from 16.3 ± 2.3 mm/year to 24.0 ± 2.9 mm/year, in consistence with the observation of Reilinger et al. (2006) that the Anatolian block is being pulled by the Hellenic trench (Fig. 1) rather than being pushed by the Arabian plate as result of continental collision between the Arabian and Eurasian plate in eastern Turkey in late Miocene (Şengör and Yılmaz, 1981). It must be noted that slip rate is not well constrained since there is no GPS station in the far field beyond about 80 km (Fig. 6).

Locking depth increases also in the same direction from 8.1 ± 3.3 km to 12.8 ± 3.9 km (Fig. 6a–c). While the shifts in the modelled faults with respect to the location of the NAFZ are negligible in profiles 2 and 3, the northward shift in the first profile (Fig. 6a) is quite significant (i.e., 15.1 ± 2.6 km). This can be attributed to the

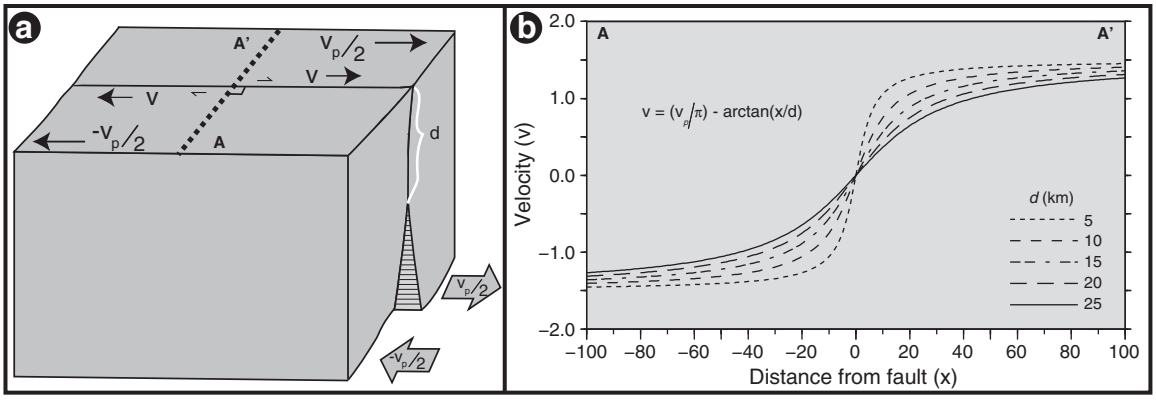

Fig. 5. A model for interseismic deformation around a plate-bounding, vertical strike-slip fault in a homogenous elastic medium: (a) Block diagram illustrating a right-lateral strike-slip fault locked from the Earth's surface to a depth of d, below which it freely slips at a constant rate equal to the relative plate motion v_p (i.e., the far field velocity). (b) Profiles of fault parallel velocity along A–A′ across the fault for various locking depths. Note the increase in the gradient of the profile around the fault with decreasing locking depth and the difference in the far field velocity on the two sides of the fault reaching to 3 cm/year at the asymptote (i.e., the rate of deep creep used in the calculations).

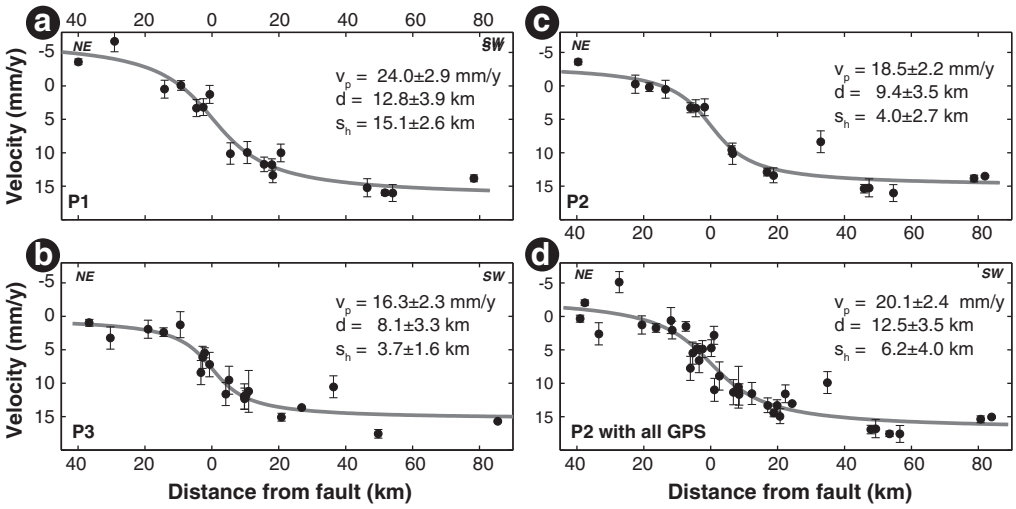

Fig. 6. Profiles of observed (GPS [black circles with error bars]) and modelled (gray thick line [the best fit]) interseismic velocities across the NAFZ. Parameters estimated by bootstrapping are shown in each profile with one σ error range. Locations of the profiles and the GPS benchmarks sampled (a, b and c) are indicated in Fig. 4. Note the increase in velocities and locking depths towards the west. An average plate velocity and locking depth in the study area is also estimated by modelling all the GPS vectors projected onto profile 2 (d).

northward right step-over of the NAFZ towards the west near Niksar (Fig. 4). A slip rate of 20.1 ± 2.4 mm/year and a locking depth of 12.5 ± 3.5 km are also estimated for the entire study area by projecting and modelling all of the GPS vectors in a single profile (Fig. 6d). Scatter plot of 500-bootstrap estimates illustrates clearly the well-known correlation, that is, trade off between the locking depth and deep slip rate (Fig. 6a) (Segall, 2002). 95% confidence limit estimated for the slip rate ranges from 16.1 mm/year to 25.9 mm/year and for locking depth from 6.7 km to 21.9 km (Fig. 7b and c).

5. Discussion and conclusions

GPS velocities across the fault segments between Niksar and Erzincan along the North Anatolian Fault Zone were calculated using campaign type GPS measurements between 2006 and 2008. The slip rate in the central part of the NAFZ located immediately to the west of the study area was estimated by Yavaşoğlu et al. (2011) to be in the range of 18.7 ± 1.6–21.5 ± 2.1 mm/year. Whereas, to the east of the study area, slip rates were deduced by Özener et al. (2010) to be in the range of 16–24 mm/year. The dextral Sungurlu fault (the Ezinepazarı-Sungurlu fault, Erturaç and Tüysüz, in press; Fig. 2) branching out from the main NAFZ as a splay fault makes a contribution to the westerly movement and rotation of the Anatolian block in different amounts according to both GPS (Yavaşoğlu et al., 2011) and paleomagnetic results (İşseven and Tüysüz, 2006; Piper et al., 1997; Tatar et al., 1995). Although the GPS results do not reveal a clear sign of contribution possibly due to the short period of observation (3 years), the paleomagnetic results obtained from the Tertiary and Quaternary volcanic rocks in the region indicate both significant clockwise and anticlockwise rotations among a vertical axis. The area between the Sungurlu Fault and the main branch of the NAFZ is dissected by active faults and the blocks bounded by secondary faults are rotated in both senses (İşseven and Tüysüz, 2006). Comparison between geodetic and geologic slip rates is rather difficult because of the reliability of the geological data (Reilinger et al., 2006).

The factors such as fault geometry within major deformation zones, presence of palaeotectonic structures and variations in fault strike, crustal thickness and locking depth may cause increase and/or decrease in the geodetic slip rates locally. However, the slip rates obtained by geological observations (20.5 ± 5.5–27 ± 7 mm/year, Hubert-Ferrari et al., 2002; Hartleb et al., 2003) are consistent with the geodetic slip rates. The North Anatolian Fault Zone located within the North Anatolian Shear Belt (Şengör et al., 2005) becomes wider especially from the western part of Kargı town centre and branch off and normal fault controlled young sedimentary basins are formed along these faults. This indicates that the transpressional character of the NAFZ along the eastern part of Niksar changes into a transtensional character along its western segments. This change is also evident along in the GPS velocity field. While GPS points on profiles 2 and 3 show generally strike slip with compressional component, to the east of profile 1 located in the central part the strike slip is dominant although the west of profile 1 covering the Niksar pull-apart basin shows strike slip with extensional component. As a matter of fact the GPS velocities in

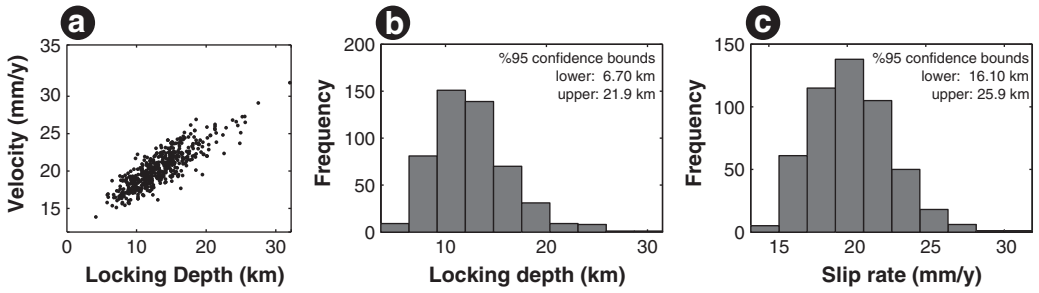

Fig. 7. (a) Scatter plot showing the trade off between slip rate and locking depth. Each point is the result of a bootstrap resample of the GPS data for 500 times using all the GPS vectors projected onto as single profile (Fig. 5d). Probability distribution for the locking depth (b) and plate velocity (c) from bootstrap results. A 95% confidence interval for each parameter is also given.

NW Anatolia indicate an increase and a change towards WSW showing the WSW escape of Anatolian block over the Aegean subduction zone.

The average slip rate obtained in this study is 20.1 ± 2.4 mm/year and compatible with the results of McClusky et al. (2000) and Reilinger et al. (2006). Slip rates, fault locking depths, shift in fault positions values were estimated on 100 km scattered and NE-SW trending 3 profiles perpendicular to the main trend of the NAFZ between Niksar and Erbaa. Slip rates of the NAFZ along these profiles from east to west are 16.3 ± 2.3 mm/year, 18.5 ± 2.2 mm/year, 24.0 ± 2.9 mm/year respectively and increase westwards. This is consistent with the findings of Yavaşoğlu et al. (2011) to the west and Özener et al. (2010) to the east of the study area.

Our analyses show that the fault locking depth increases westwards from 8.1 ± 3.3 in Erzincan to 12.8 ± 3.9 km nearby Niksar. It is estimated by Yavaşoğlu et al. (2011) to increase to 16 km further west near Ladik (Fig. 2). However, their estimation has as a large uncertainty ranging from 6 to 20 km. So, our results can be acceptable for this region. Several workers have suggested that the locking depth for the eastern part of the Sea of Marmara ranges between 10 and 15 km according to GPS and seismological data. In contrast to these studies, Meade et al. (2002) discussed the implications of low strains observed in the central and western Marmara Sea region with a block model that accounts for recoverable elastic strain accumulation. They find that GPS data can be best explained with a fairly shallow locking depth (5–6 km) on an east–west trending straight fault within the Marmara Sea. They also used the 2D screw dislocation model to calculate the locking depth and the velocity of the Ganos fault in the furthest western part of the NAFZ. The model gives the locking depth as 14 ± 7 km and velocity as 17 ± 5 mm/year. Ergintav et al. (2009) also supported the shallow locking depth in the eastern part of the Marmara Sea.

The change in locking depth from 10–16 km down to 5 km may have been caused by several rheological and seismological parameters such as thickness of the crust, rock type, geochemical composition and recent seismic activity. The wideness of deformation belt at the surface calculated by the GPS measurements on a 120 km wide belt along the Niksar–Erzincan segment of the NAFZ forming the boundary between Eurasian and the Anatolian plates varies as well. Similarly, the North Anatolian Shear Zone (NASZ, Şengör et al., 2005) including the Niksar–Erzincan segment of the NAFZ widens from east to the west (see Fig. 2, Şengör et al., 2005). The wideness of the surface deformation is calculated as 3.1 ± 1.6 km at profile 3 covering the Erzincan and its surroundings, 4.0 ± 2.7 km at profile located to the west of Suşehri and 15.1 ± 2.6 km at profile 1 including the Sungurlu fault zone and the Niksar basin. This change is also consistent with the Şengör et al. (2005) observations that the wideness of the NASZ increases towards the west. GPS results obtained from the eastern part of the NAFZ in this study are consistent with geological and fault kinematic data which also show a significant crustal movement in the region. Furthermore, these results also indicate the accumulation of interseismic deformation.

Acknowledgments

This study was carried out as part of a multidisciplinary Project (DPT 2006 120220 K) along the eastern part of the NAFZ. The Grant provided by the State Planning Organization (DPT) is greatly acknowledged. The maps in this paper were generated using the public domain Generic Mapping Tools (GMT) software (Wessel and Smith, 2001).

References

Alchalbi, A., Daoud, M., Gomez, F., McClusky, S., Reilinger, R., Romeyeh, M.A., Alsouod, A., Yassminh, R., Ballani, B., Darawcheh, R., Sbeinati, R., Radwan, Y., Masri, R.A., Bayerly, N., Ghazzi, R.A., Barazangi, M., 2010. Crustal deformation in northwestern Arabia from GPS measurements in Syria: slow slip rate along the northern Dead Sea Fault. Geophysical Journal International 180, 125–130.

Arnadottir, T., Segall, P., 1994. The 1989 Loma Prieta earthquake imaged from inversion of geodetic data. Journal of Geophysical Research 99 21, 835–21, 846.

Barka, A., Kadinsky-Cade, K., 1988. Strike–slip fault geometry in Turkey and influence on earthquake activity. Tectonics 7, 663–684.

Cakir, Z., Akoğlu, A.M., Belabbes, S., Ergintav, S., Meghraoui, M., 2005. Creeping along the Ismetpasa section of the North Anatolian Fault (Western Turkey): rate and extent from InSAR. Earth and Planetary Science Letters 238, 225–234.

Dewey, J.F., Şengör, A.M.C., 1979. Aegean and surrounding region: complex multiplate and continuum tectonics in a convergent zone. Geological Society of America Bulletin 90 (1), 84–92.

Dewey, J.F., Hempton, M.R., Kidd, W.S.F., Şaroglu, F., Şengör, A.M.C., 1986. Shortening of continental lithosphere: the neotectonics of eastern Anatolia — a young collision zone, in collision tectonics. Geological Society Special Publication 19 (3–36), 1986.

Dong, D., Herring, T.A., King, R.W., 1998. Estimating regional deformation from a combination of space and terrestrial geodetic data. Journal of Geodesy 72, 200–211.

Ergintav, S., Doğan, U., Gerstenecker, C., Çakmak, R., Belgen, A., Demirel, H., Aydın, C., Reilinger, R., 2007. A snapshot (2003–2005) of the 3D postseismic deformation for the 1999, Mw = 7.4 İzmit earthquake in the Marmara Region, Turkey, by first results of joint gravity and GPS monitoring. Journal of Geodynamics 44 (1–2), 1–18.

Ergintav, S., McClusky, S., Hearn, E., Reilinger, R., Çakmak, R., Herring, T., Özener, H., Lenk, O., Tarı, E., 2009. Seven years of postseismic deformation following the 1999, M=7.4 and M=7.2, Izmit-Düzce, Turkey earthquake sequence. Journal of Geophysical Research 114, B07403. doi:10.1029/2008JB006021.

Erturaç, M.K., Tüysüz, O., in press. Kinematics and basin formation along the Ezinepazar-Sungurlu Fault Zone, NE Anatolia, Turkey. Turkish Journal of Earth Sciences. doi:10.3906/yer-0910-27.

Farr, T.G., Rosen, P.A., Caro, E., Crippen, R., Duren, R., Hensley, S., Kobrick, M., Paller, M., Rodriguez, E., Roth, L., Seal, D., Shaffer, S., Shimada, J., Umland, J., Werner, M., Oskin, M., Burbank, D., Alsdorf, D., 2007. The shuttle radar topography mission. Reviews of Geophysics 45.

Feigl, K.L., Agnew, D.C., Bock, Y., Dong, D., Donnellan, A., Hager, B.H., Herring, T.A., Jackson, D.D., Jordan, T.H., King, R.W., Larsen, S., Larson, K.M., Murray, M.H., Shen, Z., Webb, F.H., 1993. Space geodetic measurement of crustal deformation in central and southern California, 1984–1992. Journal of Geophysical Research 98 (No B12), 21677–21712.

Hartleb, R.D., Dolan, J.F., Akyüz, H.S., Yerli, B., 2003. A 2000 year-long paleoseismologic record of earthquakes along the central North Anatolian Fault, from trenches at Alayurt, Turkey. Seismological Society of America Bulletin 93, 1935–1954.

Herece, E. and Akay E. 2003, Kuzey Anadolu Fayı (KAF) Atlası/Atlas of North Anatolian Fault (NAF). Maden Tetk. Arama Genel Müdürlüğü Özel Yayın. Ser. 2, Ankara, [IV] +61 pp.+13 appendices as separate maps

Herring, T.A., King, R.W., McClusky, S., 2006a. Documentation For The GAMIT GPS Analysis Software. Massachusetts Institute of Technology, ABD.

Herring, T.A., King, R.W., McClusky, S., 2006b. Documentation For The GLOBK GPS Analysis Software. Massachusetts Institute of Technology, ABD.

Hubert-Ferrari, A., Armijo, R., King, G., Meyer, B., Barka, A.A., 2002. Morphology, displacement, and slip rates along the North Anatolian Fault, Turkey. Journal of Geophysical Research 107 (B10), 9/1–9/33.

İşseven, T., Tüysüz, O., 2006. Palaeomagnetically defined rotations of fault bounded continental blocks in the North Anatolian Shear Zone, North Central Anatolia. Journal of Asian Earth Sciences 28, 469–479.

Jackson, J., McKenzie, D., 1988. The relationship between plate motions and seismic tremors, and the rates of active deformation in the Mediterranean and Middle East. Royal Astronomical Society Geophysical Journal 93, 45–73.

Kasapoğlu, K.E., Toksöz, M.N., 1983. Tectonic consequences of the collision of the Arabian and Eurasian Plates: finite element models. Tectonophysics 100, 71–95.

Kaypak, B., Eyidoğan, H., 2002. Erzincan havzası ve dolayının üst-kabuk hız yapısının (1-B) belirlenmesi, İTÜ Dergisi, Mühendislik Cilt:1. Sayı 2, 107–122.

Ketin, İ., 1976. San Andreas ve Kuzey Anadolu Fayları arasında bir karşılaştırma. Türkiye Jeoloji Kurumu Bülteni 19, 149–154.

Kiratzi, A.A., Papazachos, C.B., 1995. Active crustal deformation of North and East Anatolian fault zones. Tectonophysics 243 (1–24).

Kozacı, Ö., Dolan, J.F., Finkel, R., Hartleb, R., 2007. Late Holocene slip rate for the North Anatolian Fault, Turkey, from cosmogenic 36Cl geochronology: implications for the constancy of fault loading and strain release rates. Geology 35, 867–870.

McClusky, S., Balassanian, S., Barka, A., Demir, C., Ergintav, S., Georgiev, I., Gurkan, O., Hamburger, M., Hurst, K., Kahle, H., Kastens, K., Kekelidze, G., King, R., Kotzev, V., Lenk, O., Mahmoud, S., Mishin, A., Nadariya, M., Ouzounis, A., Paradissis, D., Peter, Y., Prilepin, M., Reilinger, R., Sanli, I., Seeger, H., Tealeb, A., Toksoz, M.N., Veis, G., 2000. Global Positioning System constraints on plate kinematics and dynamics in the eastern Mediterranean and Caucasus. Journal of Geophysical Research 105, 5695–5719.

McKenzie, D., 1972. Active tectonics of the Mediterranean region. Geophysical Journal of the Royal Astronomical Society 30 (2), 109–185.

Meade, B.J., Hager, B., McClusky, S.C., Reilinger, R.E., Ergintav, S., Lenk, O., Barka, A., Özener, H., 2002. Estimates of seismic potential in the Marmara Sea region from block models of secular deformation constrained by GPS measurements. Bulletin of the Seismological Society of America 92, 208–215.

Motagh, M., Hoffmann, J., Kampes, B., Baes, M., Zschau, J., 2007. Strain accumulation across the Gazikoy Saros segment of the North Anatolian Fault inferred from Persistent Scatterer Interferometry and GPS measurements. Earth and Planetary Science Letters 255, 432–444.

Oral, B., 1994. Global Positioning System (GPS) measurements in Turkey (1988–1992): Kinematics of the Africa-Arabia- Euraisa Plate collision zone, Ph.D. Thesis, 344 pp., Mass. Inst, of Technol., Cambridge.

Özener, H., Arpat, E., Ergintav, S., Dogru, A., Cakmak, R., Turgut, B., Doğan, U., 2010. Kinematics of the eastern part of the North Anatolian Fault Zone. Journal of Geodynamics 49, 141–150.
Pınar, A., Honkura, Y., Kikucki, M., 1996. A rupture model for the 1967 Mudurnu valley, Turkey earthquake and its implications for seismotectonics in the western part of the NAFZ. Geophysical Research Letters 23 (1), 29–32.
Piper, J.D.A., Moore, J., Tatar, O., Gürsoy, H., Park, R.G., 1996. Palaeomagnetic study of crustal deformation across an intracontinental transform: The North Anatolian Fault Zone in Central Turkey. In: Morris, A., Tarling, D.H. (Eds.), Palaeomagnetism and tectonics of the Mediterranean region: Geological Society of London Special Publication, 105, pp. 299–310.
Piper, J.D.A., Tatar, O., Gürsoy, H., 1997. Deformational behaviour of continental lithosphere deduced from block rotations across the North Anatolian Fault Zone in Turkey. Earth and Planetary Science Letters 150, 191–203.
Piper, J.D.A., Tatar, O., Gürsoy, H., Koçbulut, F., Mesci, B.L., 2006. Neotectonic deformation in Anatolia: a synthesis of palaeomagnetic evidence. Post Collisional Tectonics Magmatism in the Eastern Mediterranean Region. In: Dilek, Y., Pavlides, S. (Eds.), Geological Society of America, Special Paper, No 409.
Piper, J.D.A., Gürsoy, H., Tatar, O., Beck, M.E., Rao, A., Koçbulut, F., Mesci, B.L., 2009. Distributed neotectonic deformation in the Anatolides of Turkey: a paleomagnetic analysis. Tectonophysics 488 (1–4), 31–50.
Platzman, E.S., Platt, J.P., Tapırdamaz, C., Sanver, M., Rundle, C.C., 1994. Why are there no clockwise rotations along the North Anatolian Fault Zone. Journal of Geophysical Research-Solid Earth 99 (B11), 21705–21715.
Ray, J., Dong, D., Altamimi, Z., 2004. IGS reference frames: status and future improvements. GPS Solutions 8, 251–266.
Reilinger, R.E., McCLusky, S.C., Oral, M.B., King, R.W., Toksöz, M.N., 1997. Global Positioning System measurements of present-day crustal movements in the Arabia–Africa–Eurasia plate collision zone. Journal of Geophysical Research 102, 9983–9999.
Reilinger, R., McClusky, S., Vernant, P., Lawrence, S., Ergintav, S., Cakmak, R., Özener, H., Kadirov, F., Guliev, İ., Stepanyan, R., Nadariya, M., Galaktion, H., Mahmoud, S., Sakr, K., ArRajehi, A., Paradissis, D., Al-Aydrus, A., Prilepin, M., Guseva, T., Emre, E., Evren, Dmitrotsa, A., Filikov, S.V., Gomez, F., Al-Ghazzi, R., Karam, G., 2006. GPS constraints on continental deformation in the Africa–Arabia–Eurasia continental collision zone and implications for the dynamics of plate interactions. Journal of Geophysical Research 111, B05411. doi:10.1029/2005JB004051.
Şaroğlu, F., Emre, Ö., Kuşçu, I., 1992. Active fault map of Turkey. General Directorate of Mineral Research and Exploration Ankara.
Savage, J.C., Burford, R.O., 1973. Geodetic determination of relative plate motion in central California. Journal of Geophysical Research 78, 832–845.
Segall, P., 2002. Integration of geologic and geodetic estimates of fault slip rates on the San Andreas system. International Geology Review 44, 62–82.
Şengör, A.M.C., 1979. The North Anatolian transform fault: its age, offset and tectonic significance. Journal of the Geological Society 136 (3), 269–282.
Şengör, A.M.C., Yılmaz, Y., 1981. Tethyan evolution of Turkey: a plate tectonic approach. Tectonophysics 75, 181–241.
Şengör, A.M.C., Görür, N., Şaroğlu, F., 1985. Strike-slip faulting and related basin formation in zones of tectonic escape: Turkey as a case study. In: Biddle, K., Christie-Blick, N. (Eds.), Strike-slip Faulting and Basin Formation, 37. Society of Economic Paleontologists and Mineralogists, Special Publication, Tulsa, OK.
Şengör, A.M.C., Tüysüz, O., İmren, C., Sakınç, M., Eyidoğan, H., Görür, N., Le Pichon, X., Rangin, C.C., 2005. The North Anatolian fault: a new look. Annual Review of Earth and Planetary Sciences 33, 1–75.
Straub, C. 1996. Recent Crustal Deformation and Strain Accumulation in the Marmara Sea Region, N.W. Anatolia, Inferred from GPS Measurements, PhD Thesis, ETH Zürich, Switzerland.
Tapırdamaz, M.C., ve Yaltırak, C., 1996. Trakya'da Senozoyik Volkaniklerinin Paleomanyetik Özellikleri ve Bölgenin Tektonik Evrimi, MTA Dergisi. Sayı 119, 27–43.
Tatar, O., Piper, J.D.A., Graham, P.R., Gürsoy, H., 1995. Palaeomagnetic study of block rotations in the Niksar overlap region of the North Anatolian Fault Zone, central Turkey. Tectonophysics 244, 251–266.
Tatar, O., Piper, J.D.A., Gürsoy, H., Heimann, A., Koçbulut, F., 2004. Neotectonic deformation in the transition zone between the Dead Sea Transform and the East Anatolian Fault Zone, Southern Turkey: a palaeomagnetic study of the Karasu Rift Volcanism. Tectonophysics 385, 17–43.
Tatar, O., Gürsoy, H., Koçbulut, F., Kavak, K.Ş., Sezen, T.F., Polat, A., Akpınar, Z., Mesci, L., ve Kiratik, L.O., 2006. Kuzey Anadolu Fay Zonu — 1942 Erbaa-Niksar depremi yüzey kırığı: yeni gözlemler. : ATAG10, 2–4. Kasım 2010, İzmir.
Taymaz, T., Jackson, J., McKenzie, D., 1991. Active Tectonic of North and central Agean Sea. Geophysical Journal International 106, 433–490.
Wessel, P., Smith, W.H.F., 2001. The Generic Mapping Tools (GMT) Version 3.4 Technical Reference & Cookbook. SOEST/NOAA.
Yavaşoğlu, H., Tarı, E., Tüysüz, O., Çakır, Z., Ergintav, S., 2011. Determining and modeling tectonic movements along the central part of the North Anatolian Fault (Turkey) using geodetic measurements. Journal of Geodynamics 51, 339–343.